

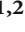

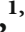





## Research Article

# Altered Coactive Micropattern Connectivity in the Default-Mode Network during the Sleep-Wake Cycle

Yan Cui <sup>1,2</sup>, Qiao Chen <sup>1,2</sup>, Yang Xia <sup>1,2</sup>, Zeru Wang <sup>1,2</sup>, Yujia Guo <sup>1,2</sup>, Ge Zhang <sup>1,2</sup>,  
Dezhong Yao <sup>1,2,3</sup> and Daqing Guo <sup>1,2</sup>

<sup>1</sup>The Clinical Hospital of Chengdu Brain Science Institute, MOE Key Lab for Neuroinformation, Center for Information in Medicine, School of Life Science and Technology, University of Electronic Science and Technology of China, Chengdu 611731, China

<sup>2</sup>Research Unit of Neuroinformation, Chinese Academy of Medical Sciences, 2019RU035, Chengdu, China

<sup>3</sup>School of Electrical Engineering, Zhengzhou University, Zhengzhou 450001, China

Correspondence should be addressed to Daqing Guo; dqguo@uestc.edu.cn

Received 31 July 2020; Revised 13 October 2020; Accepted 23 October 2020; Published 9 November 2020

Academic Editor: Rubin Wang

Copyright © 2020 Yan Cui et al. This is an open access article distributed under the Creative Commons Attribution License, which permits unrestricted use, distribution, and reproduction in any medium, provided the original work is properly cited.

The default-mode network (DMN) is believed to be associated with levels of consciousness, but how the functional connectivity (FC) of the DMN changes across different states of consciousness is still unclear. In the current work, we addressed this issue by exploring the coactive micropattern (CAMP) networks of the DMN according to the CAMPs of rat DMN activity during the sleep-wake cycle and tracking their topological alterations among different states of consciousness. Three CAMP networks were observed in DMN activity, and they displayed greater FC and higher efficiency than the original DMN structure in all states of consciousness, implying more efficient information processing in the CAMP networks. Furthermore, no significant differences in FC or network properties were found among the three CAMP networks in the waking state. However, the three networks were distinct in their characteristics in two sleep states, indicating that different CAMP networks played specific roles in distinct sleep states. In addition, we found that the changes in the FC and network properties of the CAMP networks were similar to those in the original DMN structure, suggesting intrinsic effects of various states of consciousness on DMN dynamics. Our findings revealed three underlying CAMP networks within the DMN dynamics and deepened the current knowledge concerning FC alterations in the DMN during conscious changes in the sleep-wake cycle.

## 1. Introduction

Sleep is associated with the fading of consciousness, and it is manifested objectively as a reduction in responsiveness to environmental stimuli [1, 2]. Over the past few decades, the changes in functional connectivity (FC) across multiple brain regions during sleep have been recognized as a key issue in investigating the electrophysiological mechanism of consciousness [3–5]. Brain networks always display increased dissociation of FC as deep sleep occurs [6, 7], favoring more randomized structures with lower local efficiency [8]. Moreover, segregated network modules can be observed in deep sleep [9], implying a close relationship between reduced functional integration and the loss of consciousness. One of the most studied brain networks during sleep is the default-mode network (DMN) [10–12], which is believed to be

closely related to consciousness and cognitive functions in both humans and animals [13–15]. The regions of the DMN retain their coupling during light sleep and are decoupled during deep sleep, signifying that DMN connections may support certain states of consciousness [16, 17]. In addition, the alterations in FC in DMN subsystems from light sleep to deep sleep account well for the quantitative features of light sleep [18]. However, the FC among core regions of the DMN has been found to remain intact during sleep [11]. Thus, the underlying neural mechanism of the alterations in DMN connectivity during changes in consciousness remains unclear.

Functional connectivity reflects the synchronization of neural activity in multiple brain regions, and various algorithms have been proposed to characterize it [19]. The most commonly applied measurement is the coherence algorithm

[20], which statistically describes the interdependency between pairs of time series in the frequency domain. However, the electroencephalography (EEG) signals, which reveal the electrical activity of the brain along the scalp, typically contain several distinct sources of interference and background noise that cannot be removed by artifact removal or other methods. In addition, functional magnetic resonance imaging (fMRI) can detect changes associated with blood flow (the blood oxygen level-dependent (BOLD) signals) from many brain voxels [21], but it cannot directly reveal the neural activity and also contains the background noise. All of these stochastic effects may account for spurious connectivity when connectivity is assessed with the existing methods [22, 23], which estimate the static functional connectivity. Recently, several studies have conjectured that exploring the FC patterns from the dynamic FCs of neural activity might help reveal the underlying connectivity, and several methods have been proposed, such as dynamic functional connectivity (dFC) and microstate networks. The dFC describes the FC pattern from a series of varied FC networks estimated with sliding windows [24, 25], and microstate networks indicate the FC patterns over the time points that belong to the same microstates [26, 27]. Based on these measurements, prior studies have identified novel FC patterns from brain activity and demonstrated that these FC patterns play different roles in cognitive functions [28]. Thus, depicting the FC networks from dynamic brain activity with specific joint features makes sense.

In the present study, we hypothesized that there might exist different FC structures during DMN dynamics in the sleep-wake cycle, and their alterations among distinct conscious states could help deepen our understanding about the association between DMN activity and consciousness. Accordingly, we recorded the local field potentials (LFPs) from the rat DMN during wakefulness and sleep. To derive the FC networks from rat DMN dynamics, we proposed a novel coactive micropattern network (CAMP network) method to construct the FCs among DMN regions based on the coactive micropatterns (CAMPs) from DMN dynamics described in our previous work [29]. Our results illustrated more robust functional structures of the CAMP networks than the original DMN structure, and different CAMP networks played distinct roles in specific levels of consciousness. Additionally, both CAMP networks and original DMN structures exhibited similar topological alterations during the sleep-wake cycle, indicating a homogeneous influence on DMN dynamics from the changes in consciousness and further deepening our knowledge about the relationship between the DMN and levels of consciousness.

## 2. Materials and Methods

*2.1. Experiments and Data Recording.* In the current work, 29 male Sprague-Dawley rats were used in our experiments. Fifteen electrodes were chronically implanted into the brains of rats under deep anesthesia to acquire neural activity in DMN regions. The rat DMN contained the following bilateral structures: the orbital frontal cortex (OFC), the rostral dorsal prelimbic cortex (PrL), the cingulate cortex (CG), the retro-

TABLE 1: Coordinates of the 15 DMN electrodes (mm). A-P, M-L, and D-V indicate the anterior-posterior, medial-lateral, and dorsal-ventral directions, respectively.

	A-P	M-L	D-V
The rostral dorsal prelimbic cortex (PrL)	4.2	$\pm 0.8$	3
The orbital frontal cortex (OFC)	3.7	$\pm 1.8$	4.7
The cingulate cortex (CG)	1.7	$\pm 0.7$	2.6
The retrosplenial cortex (RSC)	-3.3	0	0
The dorsal hippocampus (HIP)	-4.3	$\pm 1.4$	3
The posterior parietal cortex (PPC)	-4.5	$\pm 4$	0
The medial secondary visual cortex (V2)	-5.2	$\pm 2.4$	0
The temporal lobe (TE)	-5.2	$\pm 8$	5

splenial cortex (RSC), the dorsal hippocampus (HIP), the temporal lobe (TE), the medial secondary visual cortex (V2), and the posterior parietal cortex (PPC). The coordinates of these fifteen DMN electrodes are based on the work of Lu and his colleagues [30] and are shown in Table 1. The reference electrode was implanted in the cerebellum, and two electromyographic (EMG) electrodes were implanted bilaterally in the dorsal neck muscles. After the electrode implantation surgery, all rats were raised for at least 2 weeks for recovery before the recording session started. During the recording session, the rats were placed in a noise-attenuated chamber. The local field potentials (LFPs) from DMN regions, the EMG signals, and the simultaneous video recordings were continuously acquired for 72 h. The amplified and filtered signals (0.16–100 Hz for LFPs, 8.3–500 Hz for electromyogram (EMG), and 50 Hz notch filter) were stored on a hard disk, and the sample frequency was set to 1,000 Hz. All experimental animal procedures were approved by the Institutional Animal Care and Use Committee of the University of Electronic Science and Technology of China.

After the recording session, histological images of DMN regions for each rat were performed to confirm whether the positions of electrodes were in the correct DMN regions, especially for four deep regions. The data used in the current work is the same as that in our prior work, where we have displayed the histological images of four DMN deep regions, including the PrL, OFC, CG, and HIP. Only the rats with electrodes in accurate DMN regions were used in the current work.

The dataset used in the current study was selected from the last 24 h of the recording. We chose the dataset from the last 24 h of the recording because, at that time, the rats were more adjusted to the experimental environment and felt less external pressure during the signal acquirement. The total dataset was separated into three different conscious states, including the awake resting state (AWAKE), the slow-wave sleep state (SWS), and the rapid eye movement sleep state (REM). The data for each state were selected by several experts, and the rules for selection have been summarized in our previous publication based on the LFP, EMG, and simultaneous videos [31]. For each rat, 30 segments were chosen for different states, and each segment lasted 10 s. In total, we obtained approximately 300 s of LFPs for each rat in each conscious state.

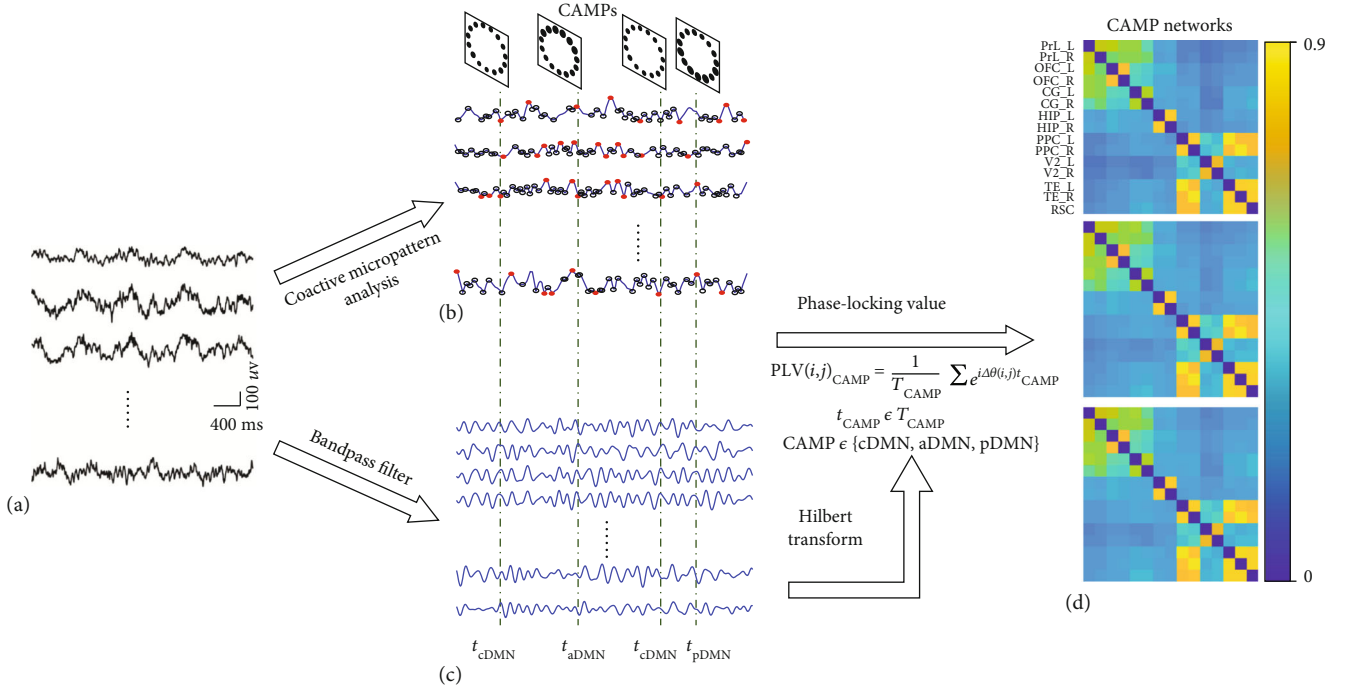


FIGURE 1: Illustration of the algorithm of CAMP networks. (a) The originally recorded signals from DMN regions. (b) The CAMPs in the dynamics of DMN activity. (c) Low-frequency bandpass-filtered signals from the original signals. In the present study, we passed the signals through a 1-4 Hz bandpass filter. (d) The three CAMP networks were identified for the three CAMPs by the PLV algorithm.

**2.2. CAMP Network Algorithm.** The coactive micropatterns (CAMPs) in DMN dynamics are the characteristic maps of DMN activity which constitute the dynamics of DMN activity, and the algorithm for extracting the CAMPs has been proposed in our recent work [29]. In the current study, we further estimated the functional connectivity network of DMN for each CAMP in DMN dynamics and tracked their alterations across different conscious states. Several steps were included in the CAMP network method.

First, we derived the CAMPs from the dynamics of DMN gamma (40-80 Hz) activity (Figure 1(b)). Electrophysiological gamma activity is believed to be strongly correlated with the blood oxygen level-dependent (BOLD) signals, and the deactivation of gamma activity in DMN regions has been observed during external tasks. The description of the CAMP algorithm as well as its functional roles in different conscious states during the sleep-wake cycle has been systematically presented in our prior work [29]. Briefly, the original DMN activity was bandpass filtered into gamma oscillation, and the Hilbert transform was then applied to obtain the envelope activity of gamma oscillation. The extreme points in the envelope activity of each DMN regions were selected as the active points. If more than seven DMN regions exhibited the extreme points at the same time, we then defined the DMN activity in all regions at that time point as the coactive pattern of DMN dynamics. Afterwards, the  $k$ -means clustering algorithm was employed to all the coactive patterns and the derived cluster centroids were the coactive micropatterns (CAMPs). Three spatially distinct CAMPs were decomposed from DMN gamma dynamics, including the common low-activity micropattern (cDMN), the anterior high-activity

micropattern (aDMN), and the posterior high-activity micropattern (pDMN). These CAMPs showed stable spatial structures during the sleep-wake cycle, and different CAMPs played distinct roles in each consciousness level. In the current work, we also focused on the CAMP index, which contained the distribution of cDMN, aDMN, and pDMN for all segments and displayed the structure of how these CAMPs constituted DMN activity. The CAMP index was applied in the next steps.

Second, the original DMN activity was low-band filtered to the delta band (1-4 Hz) to retain only the slow oscillation. It has been reported that DMN connectivity in the delta band varied during the sleep-wake cycle and played an important role in supporting conscious awareness [16, 32]. Thus, we mainly focused on the slow oscillation at the delta band in the current work. Meanwhile, the Hilbert transform was employed to this slow activity of DMN to obtain the distribution of phases in delta activity at each time point.

Third, the phase-locking value (PLV) method was used to calculate the connectivity within pairs of DMN regions for each CAMP. In detail, the phases of time points that belong to the same CAMP were concentrated, and then, the PLV method was applied to these phases to construct the structure of functional connectivity among DMN regions for each CAMP. The structure of functional connectivity for each CAMP was the CAMP network. In addition, we also estimated the functional connectivity from all time points among DMN regions, regardless of whether they belonged to the same CAMP. This functional structure was termed the original DMN structure in the further analysis.

Note that during the estimation of the CAMP network, the first step was performed for all datasets in different conscious states and 29 rats. The derived total CAMP index was then divided for each segment, state, and rat. However, the second and third steps were performed for each segment separately to obtain the structures of three CAMP networks and the original DMN structure for all segments. Finally, the CAMP network structures and original DMN structures for each rat and conscious state during the sleep-wake cycle were derived by a group averaging these four network structures estimated from the segments.

**2.3. Estimation of Topological Features for CAMP Networks through Graph Theory.** In the present study, we employed a graph theoretical analysis to characterize the properties of CAMP networks and the original DMN. This type of analysis is a mathematical approach to studying the features of complex systems, and it is designed to identify and characterize patterns in the connections between modules in a network [33].

The clustering coefficient of a network is defined as

$$C = \frac{1}{n} \sum_{i \in N} C_i = \frac{1}{n} \sum_{i \in N} \frac{\sum_{j, h \in N} (a_{ij} a_{ih} a_{jh})^{1/3}}{k_i(k_i - 1)}, \quad (1)$$

where  $a_{ij}$ ,  $a_{ih}$ , and  $a_{jh}$  are the connectivity between nodes  $i$ ,  $j$ , and  $h$  in the FC matrix  $A$ , respectively,  $N$  is the set of all nodes in the network, and  $n$  is the number of nodes.

The characteristic shortest path of a network is

$$L = \frac{1}{n} \sum_{i \in N} L_i = \frac{1}{n} \sum_{i \in N} \frac{\sum_{j \in N, j \neq i} d_{ij}^W}{n - 1}, \quad (2)$$

where  $d_{ij}^W$  is the shortest weighted path length between nodes  $i$  and  $j$ .

The small-world index of a network is measured as

$$S = \frac{C/C_{\text{rand}}}{L/L_{\text{rand}}}, \quad (3)$$

where  $C_{\text{rand}}$  and  $L_{\text{rand}}$  are the mean clustering coefficient and mean characteristic shortest path of a number of random networks derived from the tested network. In the present work, the number of random networks is 2000. Generally, we considered a network with  $S \gg 1$  to be a small-world network.

The global efficiency of a network is

$$E = \frac{1}{n} \sum_{i \in N} \frac{\sum_{j \in N, j \neq i} (d_{ij}^W)^{-1}}{n - 1}, \quad (4)$$

and the local efficiency of a network is

$$E_{\text{loc}} = \frac{1}{2} \sum_{i \in N} \frac{\sum_{j, h \in N, j \neq i} (a_{ij} a_{ih} [d_{jh}^W(N_i)]^{-1})^{1/3}}{k_i(k_i - 1)}. \quad (5)$$

Both global efficiency and local efficiency characterized the ability of information transmission in network structure [34]. Specifically, the global efficiency indicated the whole efficiency of network topological structure, while the local efficiency was the efficiency of information processing in sub-structures of the whole network and revealed the fault tolerance of the network.

Meanwhile, we estimated the network density as

$$A_{\text{mean}} = \frac{1}{n(n-1)} \sum_{i, j \in N, i \neq j} a_{ij} \quad (6)$$

to describe the connectivity of the functional network.

The synchronizability of a network features the structural property that enables the network to be synchronized, and it is expressed by the following equation:

$$\text{Syn} = \frac{\lambda_2}{\lambda_n}, \quad (7)$$

where  $\lambda_2$  is the second smallest eigenvalue of the Laplacian matrix  $L$  of the adjacency matrix  $A$ , and  $\lambda_n$  is the largest eigenvalue. A larger value of network synchronizability suggests that the network would be more synchronous [35, 36].

**2.4. Altered Rate for CAMP Networks and Original DMN across Different States.** To display the similarity of alterations in topological structures between CAMP networks and the original DMN during the sleep-wake cycle, we used the similarity features with the following equation:

$$R_{\text{sim}} = \frac{N - N_1}{N}, \quad (8)$$

where  $N_1$  is the number of connections that show the same alterations between two compared networks, such as an increase, a decrease, or no change.  $N$  is the total number of changed connections among DMN regions.

**2.5. Statistical Analysis.** In the current study, we employed Student's  $t$ -test to explore the topographic differences in FC between the CAMP networks and the original DMN in different conscious stages during wakefulness and sleep. Moreover, the difference in FC among the three conscious stages for each network was also estimated with Student's  $t$ -test. All of these tests were corrected by the familywise error (FWE) rate with  $p < 0.0002$ . In addition, to test the significant alterations in network properties between CAMP networks with the original DMN in each conscious stage, we used Student's  $t$ -test and displayed three types of significant differences for the comparisons: significant difference



( $p < 0.05$ ), very significant difference ( $p < 0.01$ ), and most significant difference ( $p < 0.001$ ).

### 3. Results

*3.1. Comparisons of Topological Structures between Three CAMP Networks and the Original DMN.* First, using the PLV method, we constructed three CAMP networks from the DMN activity for three different states of consciousness during the sleep-wake cycle based on the CAMPs we described in our prior study. Specifically, the functional network derived from the common low-activity micropattern was named the cDMN (cDMmN), the network from the aDMN was named the anterior default-mode micropattern network (aDMmN), and the network for the pDMN was named the posterior default-mode micropattern network (pDMmN). All of the CAMP networks and the original DMN showed robust functional structures with different numbers of segments (data not shown). By comparing the topological differences between the three CAMP networks with the original DMN, we observed that all of these CAMP networks displayed greater FC than the original DMN in the sleep-wake cycle (Figure 2). However, the increased FC patterns were specific to different CAMP networks and different states of consciousness. In the AWAKE state, the connections between the anterior DMN regions ((prefrontal lobe (PrL), orbitofrontal cortex (OFC), and cingulate gyrus (CG)) and the posterior DMN regions (hippocampus (HIP), posterior parietal cortex (PPC), temporal lobe (TE), V2, and retrosplenial cortex (RSC)) increased significantly in the three CAMP networks. Moreover, the cDMmN displayed enhanced FC within the posterior DMN regions while the aDMmN and pDMmN showed enhance FC within the anterior DMN regions. In the SWS state, almost all FC values among DMN regions were observed to increase in the aDMmN and pDMmN. The cDMmN displayed increased FCs between anterior DMN regions and posterior DMN regions. These differences between the increased FC in cDMmN and that in aDMmN/pDMmN suggested that the functional structure of cDMmN was more similar to the original DMN in the deep sleep state. However, in the REM sleep state, cDMmN exhibited more increased FCs than aDMmN and pDMmN, indicating that the functional structures of aDMmN and pDMmN are more similar to the functional structure of the original DMN.

Although all CAMP networks showed increased FC among DMN regions than the original DMN, several differences among them also existed. As shown in Figure 3, no difference in FCs across the three CAMP networks could be observed in the AWAKE state. In the SWS state, the cDMmN presented significantly higher FC than the aDMmN or pDMmN, especially the connections between anterior DMN regions and posterior DMN regions. Conversely, the cDMmN had lower FC than the aDMmN or pDMmN in the REM sleep state. These opposite changes revealed that the functional roles of cDMmN and aDMmN/pDMmN might be distinct for the different sleep states. Interestingly, we observed no difference in FC between the aDMmN and the pDMmN in SWS or REM

sleep, suggesting that these two CAMP networks might have similar functions during sleep.

*3.2. Comparisons of Network Properties between CAMP Networks and the Original DMN.* Network properties quantitatively represent the graphical structure and the efficiency of information transition in the network. In the current work, we first assessed the density and synchronizability of three CAMP networks and the original DMN in different states of consciousness. Consistent with the alterations in FCs among DMN regions across three levels of consciousness, the network densities of FCs in three CAMP networks were larger than that in the original DMN for all conscious states. In the two sleep states, a significant difference was observed between the network density of cDMmN and aDMmN or pDMmN. In the SWS stage, the aDMmN and pDMmN showed the largest values of network density, whereas in the REM sleep stage, the network density of the cDMmN was the largest (Figure 4(a)). Moreover, the alterations in network synchronizability in all four networks were similar to those of network density (Figure 4(b)). These similarities implied that our proposed CAMP networks were more synchronous than the original DMN.

Moreover, we estimated the small-worldness as well as the clustering coefficient and the characteristic shortest path for three CAMP networks and the original DMN in different states of consciousness. By comparison, we observed that all CAMP networks displayed larger clustering coefficients and smaller characteristic shortest paths than the original DMN during the sleep-wake cycle (Figures 5(a) and 5(b)). Meanwhile, the small-world indices of the three CAMP networks were larger than those of the original DMN, indicating that the CAMP networks had greater small-worldness than the original DMN structure (Figure 5(c)). However, in the SWS state and REM sleep state, these properties of cDMmN, aDMmN, and pDMmN were slightly distinct. As we could see, cDMmN showed a larger clustering coefficient, smaller characteristic shortest path, and larger small-world index than aDMmN or pDMmN in the SWS state. However, in the REM sleep state, aDMmN and pDMmN presented larger clustering coefficients, smaller characteristic shortest paths, and larger small-world indices than cDMmN. In addition, pDMmN displayed greater small-worldness than aDMmN in the REM sleep state due to the larger clustering coefficient, smaller characteristic shortest path, and larger small-world index.

We also estimated the efficiency of each of the three CAMP networks and the original DMN, including the global efficiency and the local efficiency. We found that both the global efficiency and the local efficiency of the three CAMP networks were greater than those of the original DMN, suggesting that the CAMP networks were more efficient. In addition, cDMmN was the most efficient structure of all networks in the SWS state, and pDMmN was the most efficient in the REM sleep state (Figure 6).

*3.3. Similar Topological Alterations in CAMP Networks and the Original DMN across Changes in Consciousness.* The FCs among DMN regions showed various topological

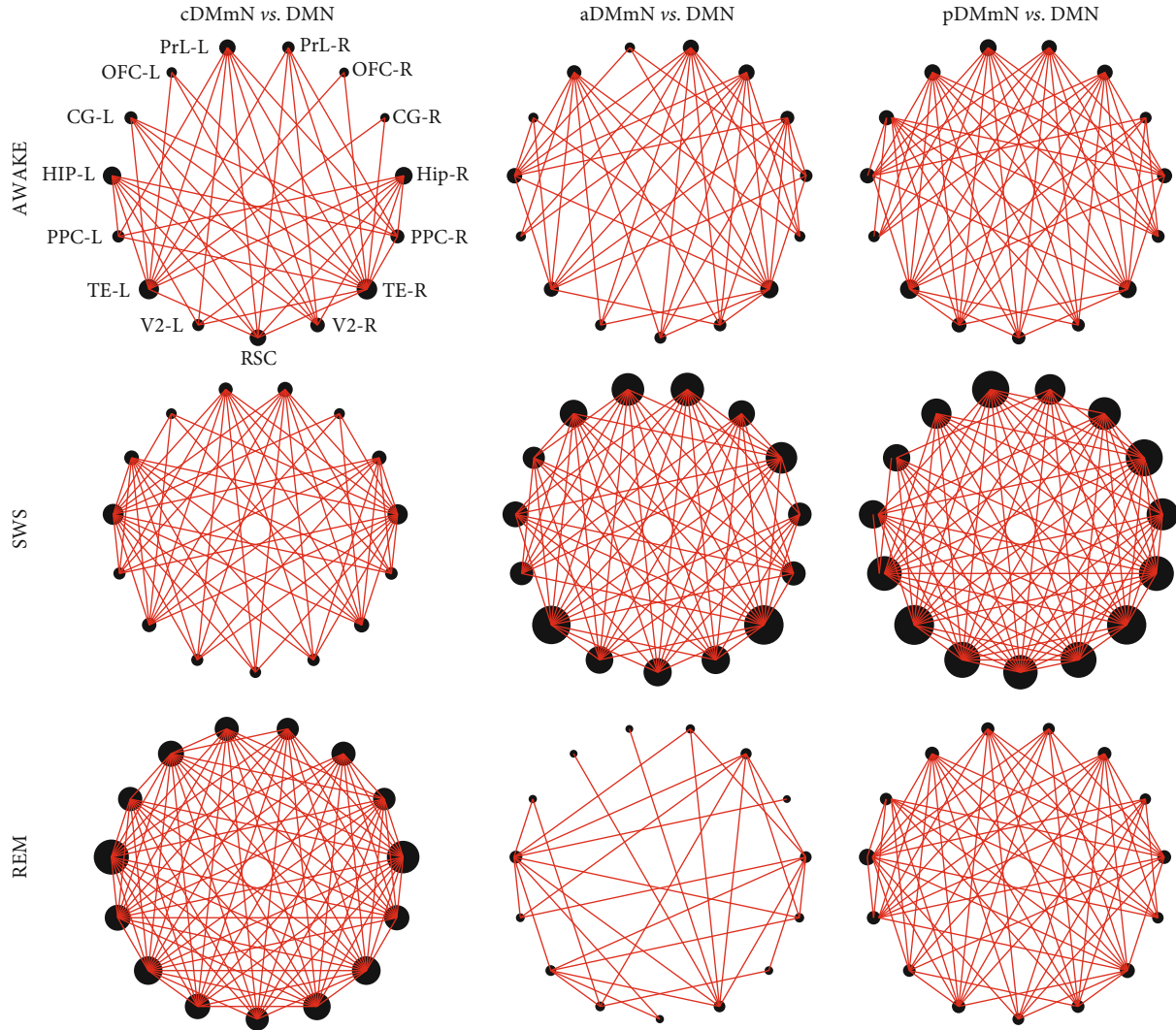


FIGURE 2: Comparisons between CAMP networks and the original DMN in different states of consciousness. The red lines indicate significantly increased FC with  $p < 0.0002$  (FWE correction).

changes across the conscious states (first row in Figure 7). Compared with the AWAKE state, the anterior DMN regions showed decreased FCs within themselves while the posterior DMN regions, except the hippocampus, displayed increased FCs in the SWS state. During the REM sleep state, the FCs within anterior DMN regions and FCs between anterior DMN regions with posterior DMN regions decreased significantly. In addition, we found that the FCs in the REM sleep state were decreased compared with those in the SWS state, especially the FCs within anterior DMN regions and within posterior DMN regions.

The alterations in FC in the three CAMP networks and the original DMN across states of consciousness were highly similar (Figure 7) and with small altered rates (Table 2). For the alterations in FCs between the AWAKE state and the SWS state, cDMmN displayed a 0.95% altered rate, and aDMmN/pDMmN showed 12.38%/4.76% altered rates to the original DMN. In addition, alterations in FCs in the cDMmN, aDMmN, and pDMmN presented 16.19%, 18.10%, and 0.95% altered rates, respectively, to those in the original

DMN when comparing the AWAKE state and the REM sleep state. The altered rates of FC changes between the three CAMP networks (cDMmN, aDMmN, and pDMmN) and the original DMN measured 4.76%, 16.19%, and 15.24%, respectively, for the comparison between the SWS state and the REM sleep state. These low altered rates and high degrees of similarity further indicated that the alterations in consciousness might respond to consistent FC variations for the DMN, including the CAMP networks. However, a slight difference was found between the alterations in FCs in aDMmN and pDMmN and those in the original DMN. In these two CAMP networks, the hippocampus showed increased FC with the temporal lobe during the SWS state, whereas no significant changes were found in the original DMN and cDMmN. In addition, greater decreases were observed in FC between the anterior DMN regions and the posterior DMN regions than between the original DMN and cDMmN in the REM sleep state. All of these differences suggested that the CAMP networks might play different roles during changes in consciousness across the sleep-wake cycle.

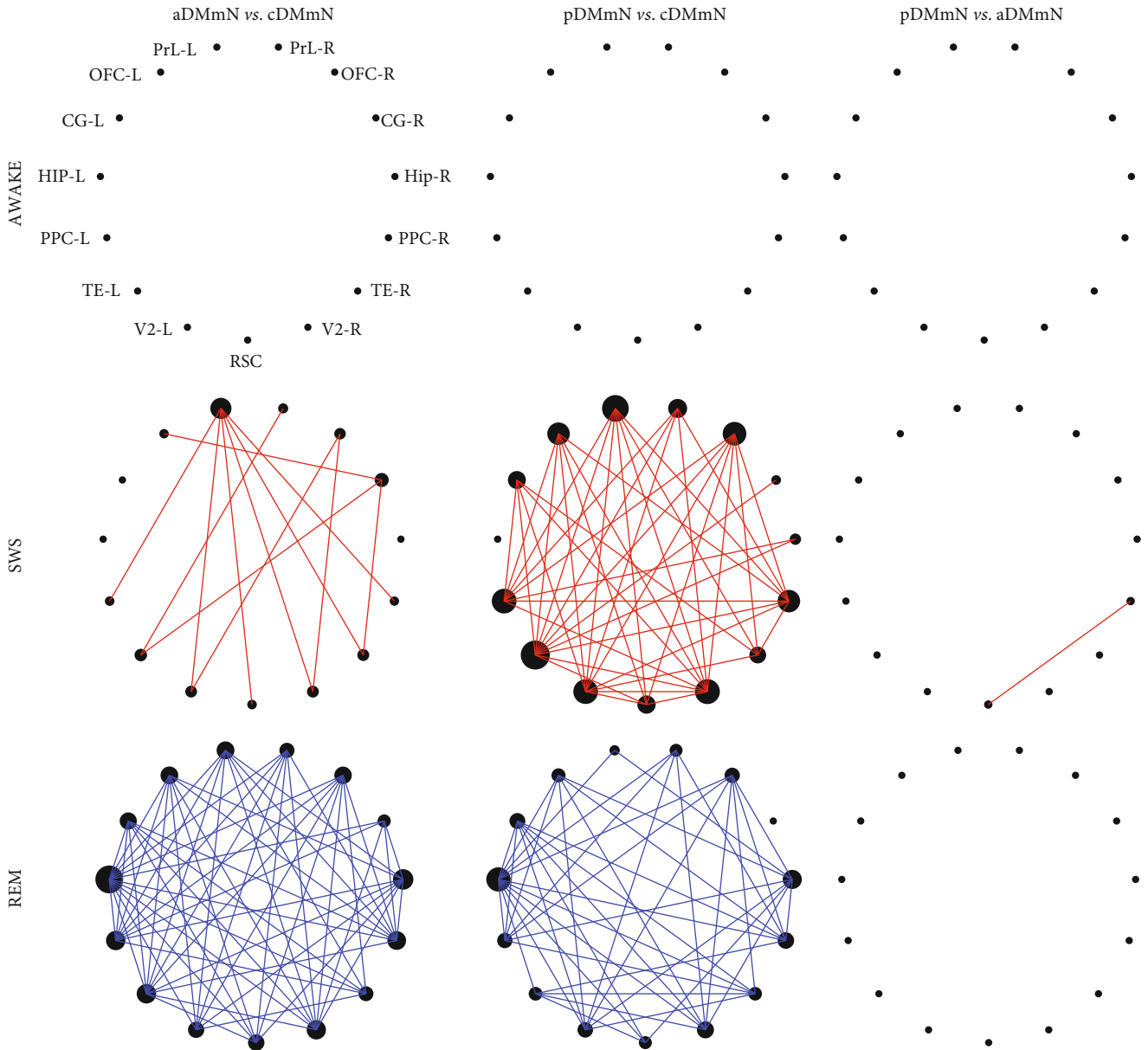


FIGURE 3: Comparisons among the three CAMP networks in different states of consciousness. The red lines indicate significantly increased FC with  $p < 0.0002$  (FWE correction). The blue lines indicate significantly decreased FC with  $p < 0.0002$  (FWE correction).

#### 4. Discussion

In the current study, we derived three CAMP networks (i.e., cDMmN, aDMmN, and pDMmN) based on CAMPs in DMN activity and compared their topological structures and properties among states of consciousness during the sleep-wake cycle. We found that all of these CAMP networks displayed increased FCs compared with the original DMN in all states of consciousness. Moreover, the local and global efficiencies were higher in the three CAMP networks than in the original DMN, suggesting that the CAMP networks executed more efficient information processing during the sleep-wake cycle. In the AWAKE state, no difference could be observed among the CAMP networks for both topological structures and features. However, the aDMmN and pDMmN

became more efficient in the SWS sleep state, whereas in the REM sleep state, the cDMmN was the most efficient structure. These differences indicated that the roles of the three CAMP networks might be specific to distinct states in sleep. Interestingly, the alterations in topological structures and features of CAMP networks were highly similar to the original DMN, implying an intrinsic effect of conscious alteration on the DMN activity. Taken together, our findings revealed the underlying functional structures of DMN activity associated with its CAMPs and deepened the current knowledge regarding the alteration in DMN FC during changes in consciousness in the sleep-wake cycle.

The FC of the DMN always changes during the sleep-wake cycle. The decoupling of frontal DMN regions with other DMN regions has been noted in the SWS state, with

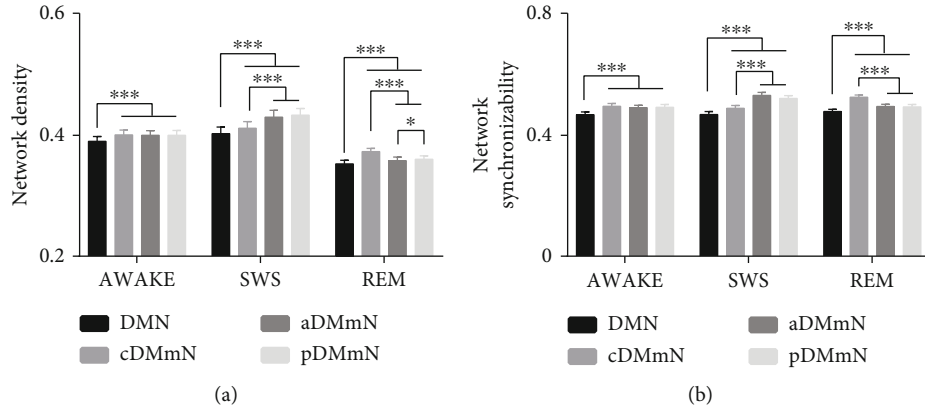


FIGURE 4: The network density of FC and network synchronizability of the three CAMP networks and the DMN in each state of consciousness. (a) Comparisons of network density. (b) Comparisons of network synchronizability. \* indicates a significant difference with  $p < 0.05$ . \*\* indicates a very significant difference with  $p < 0.01$ . \*\*\* indicates the most significant difference with  $p < 0.001$ .

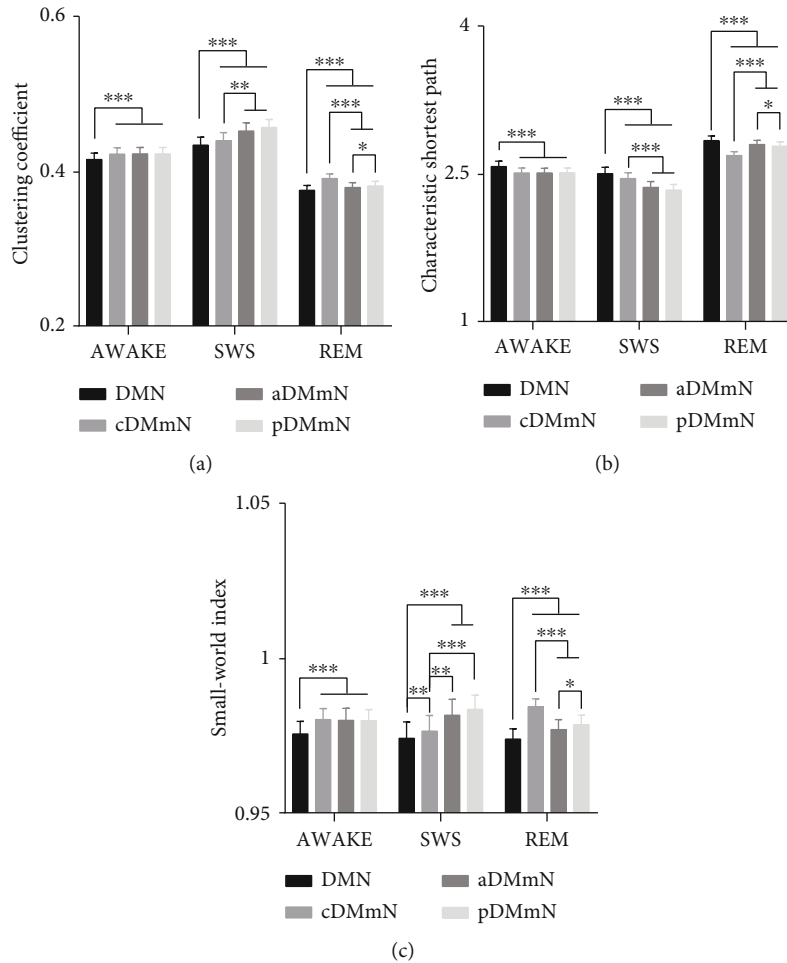


FIGURE 5: The clustering coefficients, characteristic shortest paths, and small-world indices of the three CAMP networks and the DMN in each state of consciousness. (a) Comparisons of clustering coefficients. (b) Comparisons of characteristic shortest paths. (c) Comparisons of small-world indices. \* indicates a significant difference with  $p < 0.05$ . \*\* indicates a very significant difference with  $p < 0.01$ . \*\*\* indicates the most significant difference with  $p < 0.001$ .

an increase in connectivity strength within posterior DMN regions [17, 37, 38]. Accordingly, our findings revealed that the FC strength among anterior DMN regions was reduced

while that within posterior DMN regions was significantly increased. This increase indicated a strong clustering of the posterior submodule in the DMN during deep sleep [39]



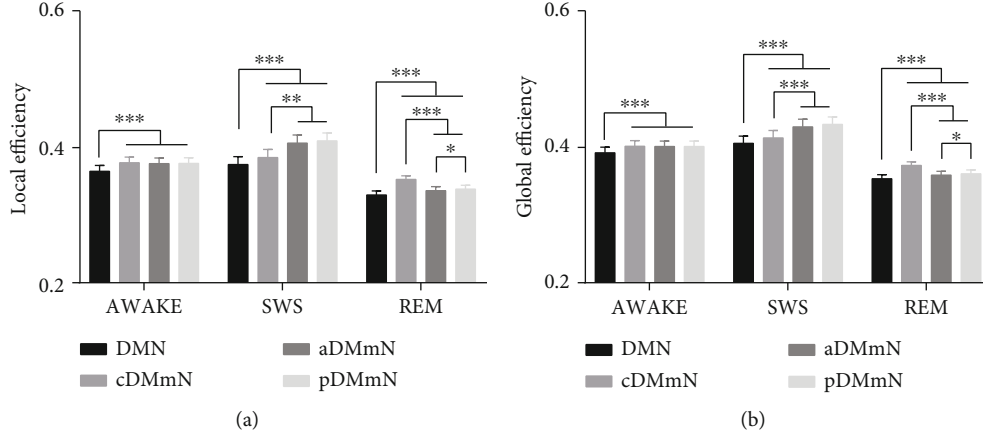


FIGURE 6: The local and global efficiency of the three CAMP networks and the DMN in each state of consciousness. (a) Comparisons of local efficiency. (b) Comparisons of global efficiency. \* indicates a significant difference with  $p < 0.05$ . \*\* indicates a very significant difference with  $p < 0.01$ . \*\*\* indicates the most significant difference with  $p < 0.001$ .

and may be related to the memory consolidation process. Memory consolidation often occurs during deep sleep [40–42], and the coupling between the hippocampus and cortical regions mediates memory consolidation during sleep [43]. We found that the pDMmN exhibited increased coupling between the HIP and TE during deep sleep, illustrating the participation of DMN neural activity in memory consolidation during deep sleep. Meanwhile, the graph theoretical analysis demonstrated an enhanced clustering coefficient and decreased characteristic shortest path of all DMmNs and DMN during the SWS state, implying a more regularized structure of the DMN in deep sleep [8]. In addition, increased network density and efficiency also emerged, suggesting that the structure of the DMN was more efficient for information processing during the deep sleep state.

However, in the REM sleep state, all of the DMN and DMmNs showed decreased connections within anterior DMN regions and within posterior DMN regions. This decrease in FC in the DMN has also been investigated in a prior study, and the opposite alteration in FCs in the DMN between the SWS state and the REM sleep state suggested that DMN activity might be modulated in distinct sleep states [44]. In addition, all of the DMmNs and the original DMN tended toward randomized structures with a decreased clustering coefficient and increased shortest path. This randomized structure of the DMN further implied a decreased efficiency of information processing during the REM sleep state [44, 45]. Through the connections of DMN regions decreased in the REM sleep state, we observed that the connectivity between anterior and posterior DMN regions persisted in all sleep states. Our findings suggested that major interactions of DMN regions existed during sleep and were in agreement with the view that the DMN preserved the functions for consciousness and cognition during the sleep-wake cycle [46].

The functional structures of DMmNs were distinct from the functional structure of the DMN in each state of consciousness in the sleep-wake cycle, with increased FCs and efficiency among all DMN regions. The increased values of connections in DMmNs might indicate the intrinsic func-

tional structures of DMN activity because the CAMP analysis decomposed the neural activity of DMN regions into several micropatterns based on their coactivation properties. This procedure could help remove the effect of noise interference on the DMN functional structure and reveal the intrinsic DMN structures. Further investigation showed that the difference between the DMmNs and the DMN connectivity was specific to the levels of consciousness. Consistent with the findings of CAMPs, the corresponding DMmNs presented similar alterations in topographical structure to the original DMN in the AWAKE state, implying their homogeneous roles in conscious awareness at rest. Nevertheless, their topological structures in SWS and REM sleep states were distinct. The aDMmN and pDMmN were more efficient and synchronous in the SWS state while the cDMmN showed efficient topology in the REM sleep state. We have previously indicated that different CAMPs play distinct roles in different conscious states. In the present study, we also found that the roles of DMmNs were specific to different levels of consciousness. Together, our findings showed several possible activity patterns for the neural activity of DMN regions, and these patterns represented different specific functions for conscious awareness. In addition, we observed that the topological alterations in DMmNs and DMN across three states of consciousness in the sleep-wake cycle were similar, with high correlations. The changes in consciousness could result in universal alterations in DMN activity, and all of the micropattern networks of DMN activity displayed consistent variations in functional structures during sleep.

Meanwhile, we also observed increased efficiency, including the global efficiency and local efficiency, during the SWS state and decreased efficiency in the REM sleep state for all the original DMN structure and CAMP networks. The increased efficiency means less energy consumption and the decreased efficiency means more energy consumption. Thus, our findings illustrated less energy consumption of DMN during the deep sleep and more energy consumption in the REM sleep and demonstrated the functional association between DMN energy cost with different conscious states. The energy cost of DMN has been reported in a prior study,

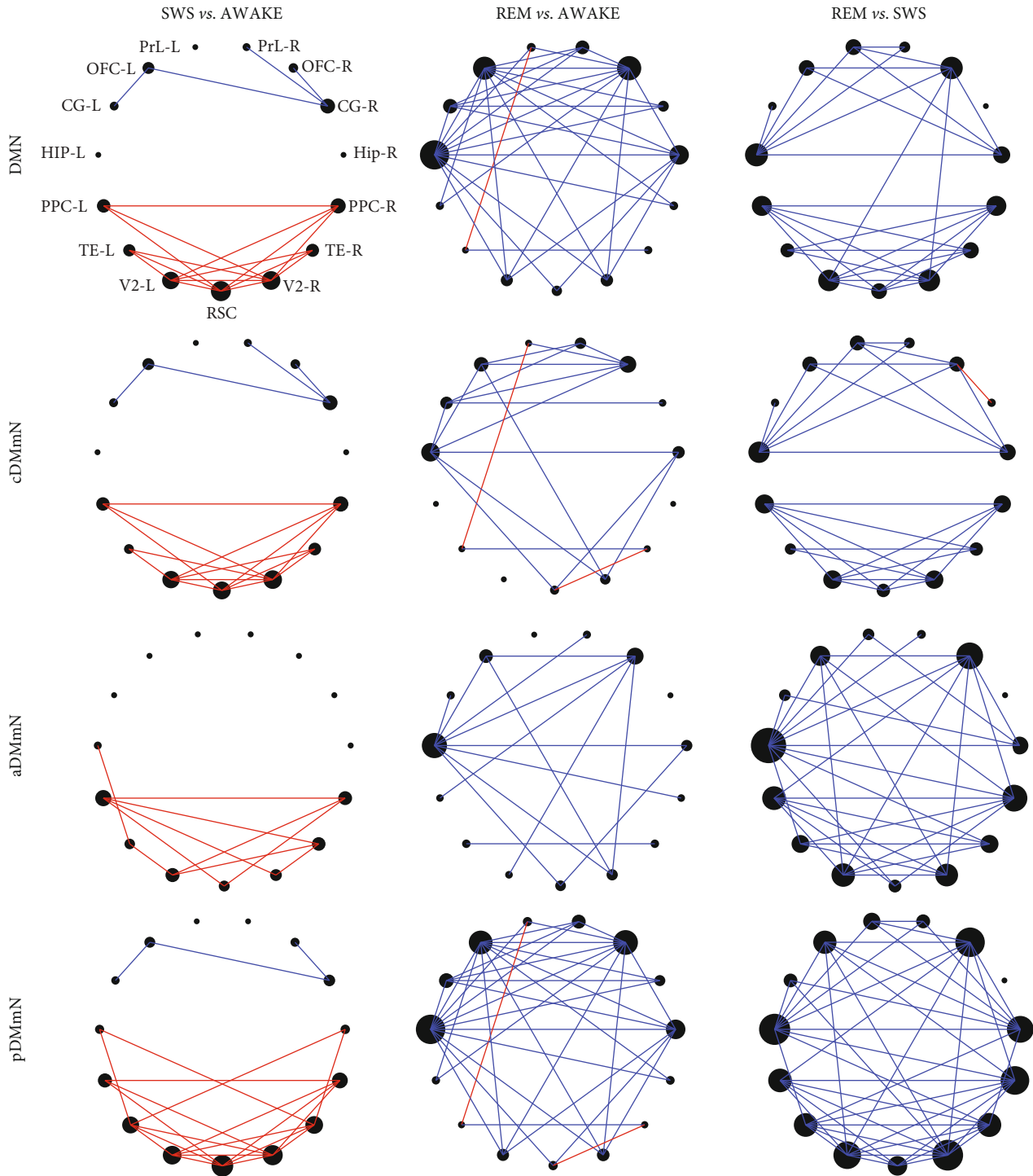


FIGURE 7: Comparisons of the three CAMP networks and the DMN among three states of consciousness. The red lines indicate significantly increased FC with  $p < 0.0002$  (FWE correction). The blue lines indicate significantly decreased FC with  $p < 0.0002$  (FWE correction).

which revealed the energy cost of DMN at the resting state and tasks using the ordinate differential equation (ODE) model [47]. Additionally, the computational models, such as the ODE model and two, have contributed to the findings of a neural mechanism for the dynamics in the sleep-wake cycle [48]. These models provided mechanistic insight into the stabilization of sleep and wake states and suggested a common underlying neural framework driving a diverse

range of observed behaviors during the sleep-wake cycle [49, 50]. Modelling sleep and the circadian cycle has been a promising way in tracking the underlying mechanism of brain activity during sleep and related disorders, which could further deepen our understanding of consciousness.

Although our findings have revealed the alterations in CAMP networks within the DMN dynamics during the sleep-wake cycle, this study also has several limitations that

TABLE 2: Altered rates between the DMN-wide FC alterations in the CAMP networks of three states of consciousness and those in the original DMN.

	AWAKE vs. SWS	AWAKE vs. REM	SWS vs. REM
cDMmN vs. DMN	0.95%	16.19%	4.76%
aDMmN vs. DMN	12.38%	19.10%	16.19%
pDMmN vs. DMN	4.76%	0.95%	15.24%

should be stated. First, our findings are based on the DMN structure of rats, which is different from that of the human brain. Although the regions of the rat DMN overlap with the regions of human DMN, our findings should be validated on human DMN activity. In addition, our DMmNs and DMN functional structures are derived from the delta band (1-4 Hz) oscillations and the CAMP points. The alterations in topological structures and features in all of these networks are specific to the frequency bands. Therefore, future investigations could reveal these alterations in the DMN functional structure in other frequency bands.

## 5. Conclusion

The alteration in DMN connections during the sleep-wake cycle is an important issue underlying the mechanism of conscious changes, and it is addressed in this work. Instead of estimating the connections among DMN regions from the whole time series, we proposed a coactive micropattern network (CAMP network) measurement that constructed the functional connection structures based on the coactive activity patterns in DMN dynamics. We found that three CAMP networks possessed distinct topological structures and graph properties in different conscious stages during the sleep-wake cycle. These differences further suggest that the roles of the three CAMP networks might be specific to distinct states in sleep. We also found that despite the differences among the three CAMP networks, the alterations in both their topological structures and graph properties were highly similar, implying an instinctive effect of conscious alteration on the dynamics of DMN activity.

## Data Availability

The data used to support the findings of this study are available from the corresponding author upon request.

## Conflicts of Interest

The authors declare that they have no conflict of interests.

## Acknowledgments

This work is supposed by the National Natural Science Foundation of China (Grant No. 31771149). This work was partly

supported by the CAMS Innovation Fund for Medical Sciences (CIFMS) (No. 2019-I2M-5-039).

## References

- [1] J. M. Windt, T. Nielsen, and E. Thompson, "Does consciousness disappear in dreamless sleep?," *Trends in Cognitive Sciences*, vol. 20, no. 12, pp. 871–882, 2016.
- [2] J. C. Claussen and U. G. Hofmann, "Sleep, neuroengineering and dynamics," *Cognitive Neurodynamics*, vol. 6, no. 3, pp. 211–214, 2012.
- [3] Y. C. Kung, C. W. Li, S. Chen et al., "Instability of brain connectivity during nonrapid eye movement sleep reflects altered properties of information integration," *Human Brain Mapping*, vol. 40, no. 11, pp. 3192–3202, 2019.
- [4] J. R. Hale, T. P. White, S. D. Mayhew et al., "Altered thalamo-cortical and intra-thalamic functional connectivity during light sleep compared with wake," *NeuroImage*, vol. 125, pp. 657–667, 2016.
- [5] D. M. Mateos, R. Guevara Erra, R. Wennberg, and J. L. Perez Velazquez, "Measures of entropy and complexity in altered states of consciousness," *Cognitive Neurodynamics*, vol. 12, no. 1, pp. 73–84, 2018.
- [6] M. Boly, M. Massimini, M. I. Garrido et al., "Brain connectivity in disorders of consciousness," *Brain Connectivity*, vol. 2, no. 1, pp. 1–10, 2012.
- [7] E. Tagliazucchi and H. Laufs, "Decoding wakefulness levels from typical fMRI resting-state data reveals reliable drifts between wakefulness and sleep," *Neuron*, vol. 82, no. 3, pp. 695–708, 2014.
- [8] V. I. Spoormaker, M. S. Schroter, P. M. Gleiser et al., "Development of a large-scale functional brain network during human non-rapid eye movement sleep," *Journal of Neuroscience*, vol. 30, no. 34, pp. 11379–11387, 2010.
- [9] E. Tagliazucchi, F. von Wegner, A. Morzelewski et al., "Large-scale brain functional modularity is reflected in slow electroencephalographic rhythms across the human non-rapid eye movement sleep cycle," *NeuroImage*, vol. 70, pp. 327–339, 2013.
- [10] S. M. Tashjian, D. Goldenberg, M. M. Monti, and A. Galván, "Sleep quality and adolescent default mode network connectivity," *Social Cognitive and Affective Neuroscience*, vol. 13, no. 3, pp. 290–299, 2018.
- [11] P. G. Sämann, R. Wehrle, D. Hoehn et al., "Development of the brain's default mode network from wakefulness to slow wave sleep," *Cerebral Cortex*, vol. 21, no. 9, pp. 2082–2093, 2011.
- [12] T. Koike, S. Kan, M. Misaki, and S. Miyauchi, "Connectivity pattern changes in default-mode network with deep non-REM and REM sleep," *Neuroscience Research*, vol. 69, no. 4, pp. 322–330, 2011.
- [13] M. E. Raichle, "The Brain's default mode network," *Annual Review of Neuroscience*, vol. 38, no. 1, pp. 433–447, 2015.
- [14] M. E. Raichle, A. M. MacLeod, A. Z. Snyder, W. J. Powers, D. A. Gusnard, and G. L. Shulman, "A default mode of brain function," *Proceedings of the National Academy of Sciences of the United States of America*, vol. 98, no. 2, pp. 676–682, 2001.
- [15] Y. Cui, S. Yu, T. Zhang et al., "Altered activity and information flow in the default mode network of pilocarpine-induced epilepsy rats," *Brain Research*, vol. 1696, pp. 71–80, 2018.

- [16] S. G. Horowitz, A. R. Braun, W. S. Carr et al., "Decoupling of the brain's default mode network during deep sleep," *Proceedings of the National Academy of Sciences of the United States of America*, vol. 106, no. 27, pp. 11376–11381, 2009.
- [17] A. Vanhaudenhuyse, Q. Noirhomme, L. J. F. Tshibanda et al., "Default network connectivity reflects the level of consciousness in non-communicative brain-damaged patients," *Brain*, vol. 133, no. 1, pp. 161–171, 2010.
- [18] C. W. Wu, P.-Y. Liu, P.-J. Tsai et al., "Variations in connectivity in the sensorimotor and default-mode networks during the first nocturnal sleep cycle," *Brain Connectivity*, vol. 2, no. 4, pp. 177–190, 2012.
- [19] H. E. Wang, C. G. Bénar, P. P. Quilichini, K. J. Friston, V. K. Jirsa, and C. Bernard, "A systematic framework for functional connectivity measures," *Frontiers in Neuroscience*, vol. 8, pp. 1–22, 2014.
- [20] J. Geweke, "Measurement of linear dependence and feedback between multiple time series," *Journal of the American Statistical Association*, vol. 77, no. 378, pp. 304–313, 1982.
- [21] N. K. Logothetis, "The neural basis of the blood-oxygen-level-dependent functional magnetic resonance imaging signal," *Philosophical Transactions of the Royal Society B: Biological Sciences*, vol. 357, no. 1424, pp. 1003–1037, 2002.
- [22] M. A. Kramer, U. T. Eden, S. S. Cash, and E. D. Kolaczyk, "Network inference with confidence from multivariate time series," *Physical Review E - Statistical, Nonlinear, and Soft Matter Physics*, vol. 79, no. 6, pp. 1–13, 2009.
- [23] L.-E. Martinet, M. A. Kramer, W. Viles et al., "Robust dynamic community detection with applications to human brain functional networks," *Nature Communications*, vol. 11, no. 1, article 2785, 2020.
- [24] E. A. Allen, E. Damaraju, S. M. Plis, E. B. Erhardt, T. Eichele, and V. D. Calhoun, "Tracking whole-brain connectivity dynamics in the resting state," *Cerebral Cortex*, vol. 24, no. 3, pp. 663–676, 2014.
- [25] W. Tang, H. Liu, L. Douw et al., "Dynamic connectivity modulates local activity in the core regions of the default mode network," *Proceedings of the National Academy of Sciences of the United States of America*, vol. 114, no. 36, pp. 9713–9718, 2017.
- [26] C. M. Michel and T. Koenig, "EEG microstates as a tool for studying the temporal dynamics of whole-brain neuronal networks: a review," *NeuroImage*, vol. 180, Part B, pp. 577–593, 2018.
- [27] R. D. Pascual-Marqui, D. Lehmann, P. Faber et al., "The resting microstate networks (RMN): cortical distributions, dynamics, and frequency specific information flow," pp. 1–14, 2014, <http://arxiv.org/abs/1411.1949>.
- [28] C. Rosazza and L. Minati, "Resting-state brain networks: literature review and clinical applications," *Neurological Sciences*, vol. 32, no. 5, pp. 773–785, 2011.
- [29] Y. Cui, M. Li, B. Biswal et al., "Dynamic Configuration of Coactive Micropatterns in the Default Mode Network during Wakefulness and Sleep," bioRxiv, 2020.
- [30] H. Lu, Q. Zou, H. Gu, M. E. Raichle, E. A. Stein, and Y. Yang, "Rat brains also have a default mode network," *Proceedings of the National Academy of Sciences of the United States of America*, vol. 109, no. 10, pp. 3979–3984, 2012.
- [31] W. Jing, D. Guo, Y. Zhang et al., "Reentrant information flow in electrophysiological rat default mode network," *Frontiers in Neuroscience*, vol. 11, no. 2, pp. 1–12, 2017.
- [32] M. Lee, B. Baird, O. Gosseries et al., "Connectivity differences between consciousness and unconsciousness in non-rapid eye movement sleep: a TMS-EEG study," *Scientific Reports*, vol. 9, no. 5175, pp. 2082–2093, 2019.
- [33] M. Rubinov and O. Sporns, "Complex network measures of brain connectivity: uses and interpretations," *NeuroImage*, vol. 52, no. 3, pp. 1059–1069, 2010.
- [34] E. Bullmore and O. Sporns, "Complex brain networks: graph theoretical analysis of structural and functional systems," *Nature Reviews Neuroscience*, vol. 10, pp. 186–198, 2009.
- [35] E. van Dellen, L. Douw, A. Hillebrand et al., "MEG network differences between low- and high-grade glioma related to epilepsy and cognition," *PLoS One*, vol. 7, no. 11, article e50122, 2012.
- [36] K. A. Schindler, S. Bialonski, M.-T. Horstmann, C. E. Elger, and K. Lehnertz, "Evolving functional network properties and synchronizability during human epileptic seizures," *Chaos*, vol. 18, no. 3, article 033119, 2008.
- [37] L. E. Mak, L. Minuzzi, G. MacQueen, G. Hall, H. S. Kennedy, and R. Milev, "The Default Mode Network in Healthy Individuals: A Systematic Review and Meta-Analysis," *Brain Connectivity*, vol. 7, no. 1, pp. 25–33, 2017.
- [38] L. J. Larson-Prior, J. M. Zempel, T. S. Nolan, F. W. Prior, A. Snyder, and M. E. Raichle, "Cortical network functional connectivity in the descent to sleep," *Proceedings of the National Academy of Sciences of the United States of America*, vol. 106, no. 11, pp. 4489–4494, 2009.
- [39] V. I. Spoormaker, P. M. Gleiser, and M. Czisch, "Frontoparietal connectivity and hierarchical structure of the brain's functional network during sleep," *Frontiers in Neurology*, vol. 3, pp. 1–10, 2012.
- [40] Y. Wei, G. P. Krishnan, M. Komarov, and M. Bazhenov, "Differential roles of sleep spindles and sleep slow oscillations in memory consolidation," *PLoS Computational Biology*, vol. 14, no. 7, article e1006322, 2018.
- [41] H. Zhang, J. Fell, and N. Axmacher, "Electrophysiological mechanisms of human memory consolidation," *Nature Communications*, vol. 9, no. 1, article 4103, 2018.
- [42] Y. Wei, G. P. Krishnan, and M. Bazhenov, "Synaptic mechanisms of memory consolidation during sleep slow oscillations," *Journal of Neuroscience*, vol. 36, no. 15, pp. 4231–4247, 2016.
- [43] N. Maingret, G. Girardeau, R. Todorova, M. Goutierre, and M. Zugaro, "Hippocampo-cortical coupling mediates memory consolidation during sleep," *Nature Neuroscience*, vol. 19, no. 7, pp. 959–964, 2016.
- [44] T. Watanabe, S. Kan, T. Koike et al., "Network-dependent modulation of brain activity during sleep," *NeuroImage*, vol. 98, pp. 1–10, 2014.
- [45] T. Uehara, T. Yamasaki, T. Okamoto et al., "Efficiency of a "small-world" brain network depends on consciousness level: a resting-state fMRI study," *Cerebral Cortex*, vol. 24, no. 6, pp. 1529–1539, 2014.
- [46] E. Tagliazucchi and E. J. W. van Someren, "The large-scale functional connectivity correlates of consciousness and arousal during the healthy and pathological human sleep cycle," *NeuroImage*, vol. 160, pp. 55–72, 2017.
- [47] X. Cheng, Y. Yuan, Y. Wang, and R. Wang, "Neural antagonistic mechanism between default-mode and task-positive networks," *Neurocomputing*, vol. 417, pp. 74–85, 2020.



- [48] J. H. Abel, K. Lecamwasam, M. A. St Hilaire, and E. B. Klerman, "Recent advances in modeling sleep: from the clinic to society and disease," *Current Opinion in Physiology*, vol. 15, pp. 37–46, 2020.
- [49] A. J. K. Phillips and P. A. Robinson, "Sleep deprivation in a quantitative physiologically based model of the ascending arousal system," *Journal of Theoretical Biology*, vol. 255, no. 4, pp. 413–423, 2008.
- [50] K. S. Williams and C. G. Diniz Behn, "Dynamic interactions between orexin and dynorphin may delay onset of functional orexin effects: a modeling study," *Journal of Biological Rhythms*, vol. 26, no. 2, pp. 171–181, 2011.